

# Diffuse ionized gas toward $\beta$ Canis Majoris <sup>\*</sup>

Olivier Dupin, Cécile Gry

Laboratoire d'Astronomie Spatiale, B.P.8, 13376 Marseille cedex 12, France, (odupin@astrsp-mrs.fr, cecile@astrsp-mrs.fr)

Received ; accepted

**Abstract.** This paper presents the study of the interstellar medium toward  $\beta$  CMa, a disk sight-line known for its low neutral gas density. This study uses high and medium resolution HST-GHRS spectra including lines from the following species : H I, D I, N I, O I, S II, S III, Si II, Si III, Si IV, Al II, Al III, Fe II, Mg I, Mg II, Mn II, C II and C IV.

The line of sight to  $\beta$  CMa (153 pc) is dominated by two ionized regions with a velocity difference of 10 km s<sup>-1</sup>. The ionized regions account for most of the total hydrogen column density, around  $2 \cdot 10^{19}$  cm<sup>-2</sup>, and the neutral gas represents only 10% of the total gas. The two ionized clouds display characteristics of the warm diffuse gas detected in the disk and the halo. Their gas-phase abundances indicate that their depletion is low, especially for the more ionized of the two clouds.

Special models of photoionization by the two EUV-excess stars  $\beta$  CMa and  $\epsilon$  CMa would be needed for a detailed discussion of the ionizing mechanisms of the clouds ; their ionization ratios are nevertheless roughly compatible with collisional ionization at temperatures around 20 000 K, substantially higher than the kinetic temperatures derived from the line widths. Their characteristics suggest that the clouds may be in the process of cooling down and recombining after having been shocked and ionized by some violent events, possibly related to the Local Bubble formation.

**Key words:** ISM: abundances – ISM: atoms – ISM: clouds – ISM: bubbles – stars:  $\beta$  CMa – ultraviolet: ISM

## 1. Introduction

Observations of the interstellar medium toward nearby stars show that the Sun is located in an interstellar void, often called the Local Bubble, filled with a hot ( $10^6$  K) and low density ( $5 \cdot 10^{-3}$  cm<sup>-3</sup>) gas, responsible for part

*Send offprint requests to:* O. Dupin

<sup>\*</sup> Based on observations with the NASA/ESA *Hubble Space Telescope*, obtained at the Space Telescope Institute, which is operated by the Association of Universities for Research in Astronomy, Inc., under NASA contract NAS5-26555.

of the soft X-ray background (e.g. Cox & Reynolds 1987 and references therein). The Bubble is irregularly shaped (Frish & York 1983), extending to at least 50 pc in most directions. *Copernicus* observations (Gry et al. 1985) have shown an extension of the Bubble as far as the star  $\beta$  CMa ( $l = 226^\circ$ ,  $b = -14^\circ$ ) 153 pc from the Sun (Hipparcos catalog). They report a neutral hydrogen column density from 1.0 to  $2.2 \cdot 10^{18}$  cm<sup>-2</sup>, and a strongly ionized sight-line. Welsh (1991) and Welsh et al. (1994), have observed the Na I line toward many neighbouring stars and confirmed the existence of this low density tunnel, 300 pc long and 50 pc wide, in the direction of  $\beta$  CMa.

More recently, Gry et al. (1995) analysed the UV absorption lines of the interstellar medium in the direction of  $\epsilon$  CMa ( $l = 239.8^\circ$ ,  $b_{II} = -11.3^\circ$ ), 132 pc from the Sun. They have shown that the absorption lines are principally due to local matter : the Local Interstellar Cloud (LIC) in which the Sun is embedded (see Lallement & Bertin 1992) as well as a cloud already detected toward the very nearby (2.7 pc) star  $\alpha$  CMa (Lallement et al. 1994), and they conclude that beyond three parsecs, the mean gas density is less than  $4.5 \cdot 10^{-4}$  cm<sup>-3</sup>. This makes this line of sight the most devoid region in the nearby interstellar medium. They also detected high ionization species like C IV, attributed to the thermal conductive interface with the hot gas, thereby observed for the first time around two nearby diffuse clouds.

Observations of  $\epsilon$  and  $\beta$  CMa have been performed in the extreme UV with the *EUVE* spacecraft. Due to their location in the tunnel and their EUV excess,  $\epsilon$  CMa and  $\beta$  CMa are respectively the first and the second brightest EUV sources in the sky, and the principal photoionization sources in the solar neighbourhood : Vallerga & Welsh (1995) have found a local interstellar hydrogen photoionization rate for  $\epsilon$  CMa seven times greater than previous estimates calculated for all nearby stars (Bruhweiler & Cheng 1988). Modelling the EUV stellar spectra, Cassinelli et al. (1995) and Cassinelli et al. (1996) found interstellar neutral hydrogen column densities of  $1.0 \cdot 10^{18}$  cm<sup>-2</sup> and  $2.0 \pm 0.2 \cdot 10^{18}$  cm<sup>-2</sup> respectively for  $\epsilon$  CMa and  $\beta$  CMa, confirming the Gry et al. (1985) result for  $\beta$  CMa.

**Table 1.** Observed spectral ranges and atomic lines.

range (Å)	element	wavelength (Å)	$f$ -value
Ech-B data			
1805.0 – 1814.6	Si II	1808.013	$2.0 \cdot 10^{-3}$
1841.6 – 1875.8	Al III	1854.716	$5.6 \cdot 10^{-1}$
	Al III	1862.789	$2.8 \cdot 10^{-1}$
2338.5 – 2350.7	Fe II	2344.214	$1.1 \cdot 10^{-1}$
2371.8 – 2383.5	Fe II	2374.461	$2.8 \cdot 10^{-2}$
	Fe II	2382.765	$3.0 \cdot 10^{-1}$
2573.9 – 2586.9	Mn II	2576.877	$3.5 \cdot 10^{-1}$
2792.1 – 2807.1	Mg II	2796.352	$6.1 \cdot 10^{-1}$
	Mg II	2803.531	$3.1 \cdot 10^{-1}$
2846.7 – 2860.7	Mg I	2852.964	$1.8 \cdot 10^0$
G160M data			
1185.7 – 1221.9	S III	1190.208	$2.2 \cdot 10^{-2}$
	Si II	1190.416	$2.5 \cdot 10^{-1}$
	Si II	1193.290	$5.0 \cdot 10^{-1}$
	N I	1199.550	$1.3 \cdot 10^{-1}$
	N I	1200.223	$8.8 \cdot 10^{-2}$
	N I	1200.710	$4.4 \cdot 10^{-2}$
	Si III	1206.500	$1.7 \cdot 10^0$
	D I	1215.339	$4.2 \cdot 10^{-1}$
	H I	1215.670	$4.2 \cdot 10^{-1}$
	1229.8 – 1265.9	S II	1250.584
S II		1253.811	$1.1 \cdot 10^{-2}$
S II		1259.519	$1.6 \cdot 10^{-2}$
Si II		1260.422	$1.0 \cdot 10^0$
1300.1 – 1336.0	O I	1302.168	$4.9 \cdot 10^{-2}$
	Si II	1304.370	$1.5 \cdot 10^{-1}$
	C II	1334.532	$1.3 \cdot 10^{-1}$
1390.4 – 1426.2	Si IV	1393.755	$5.1 \cdot 10^{-1}$
	Si IV	1402.770	$2.6 \cdot 10^{-1}$
1524.1 – 1559.3	Si II	1526.707	$2.3 \cdot 10^{-1}$
	C IV	1548.195	$1.9 \cdot 10^{-1}$
	C IV	1550.770	$9.5 \cdot 10^{-2}$
1644.4 – 1679.3	Al II	1670.787	$1.8 \cdot 10^0$

We present a study of the line of sight toward the B1 II-III star  $\beta$  CMa, performed with ultraviolet spectra of the star. Our purpose is to give a description of the structure and physical conditions of the ionized gas detected with Copernicus (Gry et al. 1985), and thereby discuss the nature of diffuse clouds embedded in the Local Bubble.

Section 2 presents the data and describes their processing. In Sect. 3 a description of the line of sight toward  $\beta$  CMa is given based on high and medium resolution data, and column densities and  $b$ -values are derived for each studied element and for each velocity component wherever possible. Section 4 deals with the physical conditions in the clouds. The ionization of the clouds is treated in Sect. 5 and the gas phase abundances in Sect. 6. In Sect. 7, the nature of the gas is discussed in comparison with other observations.

## 2. Observations and data reduction

The observations described here have been obtained in December 1992 with the Goddard High Resolution Spectrometer (GHRS) on board the Hubble Space Telescope (HST) by Vidal-Madjar and collaborators. All lines above 1800 Å have been observed with Ech-B, and have a resolution of 85 000 giving a velocity resolution of about  $3.5 \text{ km s}^{-1}$ . Because of the failure of Ech-A at that time, the short wavelength observations were made with the G160M, which gives a resolution of 20 000 and a velocity resolution of  $15 \text{ km s}^{-1}$ . Table 1 lists the observed spectral ranges and the spectral lines analysed.

All data were taken with the  $0''.25$  small science aperture (SSA), the procedure FP-SPLIT = 4 and a sub-stepping of 2 samples per diode width (for details of the instrumentation see Duncan 1992). For data processing, standard STSDAS procedures of the IRAF software were used. Wavelengths were assigned from the standard calibration tables. An error of  $\pm 1$  resolution element on the wavelength assignment is expected because of magnetic drift. We made use of an absorption line profile fitting software developed by Vidal-Madjar et al. (1977) also described in Ferlet et al. (1980a,b), and we checked our technique by comparing the results obtained with similar software developed by Welty (see Welty et al. 1991). Stellar lines were fitted with a low-order polynomial on both sides of each line and each interstellar absorption component was represented by the convolution of a theoretical Voigt profile with the instrumental profile. An iterative procedure which minimizes the quadratic differences between the profile and the data points allows to determine the column density of the absorbing elements  $N$  ( $\text{cm}^{-2}$ ), the radial velocity of the cloud ( $\text{km s}^{-1}$ ) and the line  $b$ -value ( $\text{km s}^{-1}$ ) of each interstellar absorption component. The instrumental profile is taken from Duncan (1992) and the atomic parameters from Morton (1991) except for the Si II 1808 line oscillator strength which comes from Bergeon & Lawler (1993).

## 3. Analysis

### 3.1. The structure of the sight-line : Ech-B data

The high resolution ( $\sim 3.5 \text{ km s}^{-1}$ ) of the Ech-B data allows us to determine the velocity structure of the sight-line. Two main components are clearly visible in all studied lines (Fig. 1). Two smaller features are detected only in the four strongest lines Fe II 2344, Fe II 2382, Mg II 2796 and Mg II 2803 (Fig. 1). These components are labelled A, B, C and D in order of increasing velocity.

In the analysis, the velocity shifts between components are constrained to be the same for all lines but the absolute velocities are allowed to vary slightly from one line to another to account for the uncertainty mentioned in Sect. 2. The derived velocities all lie within a range of  $\pm 1.5 \text{ km s}^{-1}$ . The average of these velocities is therefore

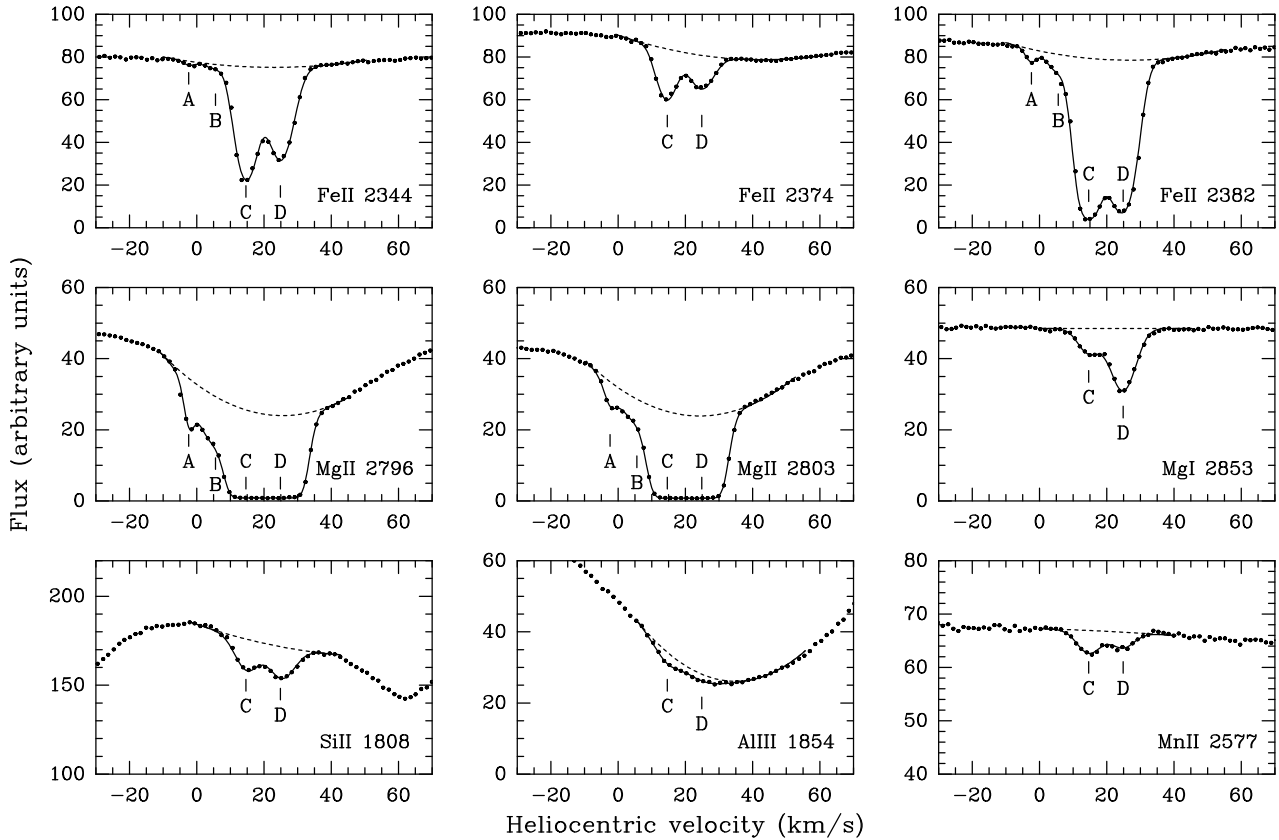


**Fig. 1.** Ech-B spectra of  $\beta$  CMA ( $R \sim 85\,000$ ). The points are the observations, the dashed lines the assumed stellar continua and the solid lines the fits to the interstellar absorption profiles. Column densities and  $b$ -values used for the fits are given in Table 2.

adopted, giving  $-2.5$ ,  $5.5$ ,  $14.5$  and  $25\text{ km s}^{-1}$  for A, B, C and D respectively, and the spectra are shifted accordingly. The above velocities thus define the heliocentric velocities of the components with an absolute precision of  $3\text{ km s}^{-1}$ .

The Sun is known to be embedded in the Local Interstellar Cloud which is moving relative to it at a velocity of  $26\text{ km s}^{-1}$  towards the direction  $l = 186^\circ$ ,  $b = -16^\circ$  (Lallement & Bertin 1992). The projection of its velocity vector on the  $\beta$  CMA direction gives  $20.3\text{ km s}^{-1}$ . This falls between component C and component D : the absorption line due to the LIC is hidden and its study is therefore impossible at the resolution of the present data. It is nevertheless taken into account in the fit with the column density and  $b$ -value found by Gry et al. (1995) toward  $\epsilon$  CMA. Another small component is present in the lines of sight of both  $\alpha$  CMA ('blue component', Lallement et al. 1994) and  $\epsilon$  CMA ('component 2', Gry et al. 1995). Because of the vicinity of the  $\alpha$  CMA and  $\beta$  CMA sight-lines, this cloud is likely to be present in the line of sight to

$\beta$  CMA and it is also taken into account in the fit with the  $\epsilon$  CMA column densities and  $b$ -values.

The component column densities and  $b$ -values are determined for all observed elements with the absorption profile fitting program mentioned in Sect. 2. All the lines of an ion are fitted simultaneously. The results are shown in Table 2. The error bars given take into account the uncertainties in the stellar continuum modeling, the velocity positions of the components and the parameters of the hidden components (LIC and  $\epsilon$  CMA component 2) as well as the statistical error of the data.

### 3.1.1. The Fe II and Mn II lines

The three lines of Fe II have different oscillator strengths and two of them are not saturated, thus they allow a reliable determination of the column density and  $b$ -value of each component. The interstellar features are superimposed on weak stellar lines which can be easily modeled by polynomials. The Mn II 2577 line is very weak, but the C and D components are clearly present. It lies in an

**Table 2.** Column densities and  $b$ -values of the individual clouds derived from the Ech-B spectra and when possible from the G160M data.

Cloud Vel.	A $-2.5 \text{ km s}^{-1}$		B $5.5 \text{ km s}^{-1}$		C $14.5 \text{ km s}^{-1}$		D $25 \text{ km s}^{-1}$	
	$N \text{ (cm}^{-2}\text{)}$	$b \text{ (km s}^{-1}\text{)}$	$N \text{ (cm}^{-2}\text{)}$	$b \text{ (km s}^{-1}\text{)}$	$N \text{ (cm}^{-2}\text{)}$	$b \text{ (km s}^{-1}\text{)}$	$N \text{ (cm}^{-2}\text{)}$	$b \text{ (km s}^{-1}\text{)}$
Fe II	$1.4 \pm 0.4 \cdot 10^{11}$	$1.7 \pm 0.8$	$3.0 \pm 0.1 \cdot 10^{11}$	$2.8 \pm 0.7$	$1.2 \pm 0.1 \cdot 10^{13}$	$3.6 \pm 0.1$	$1.0 \pm 0.1 \cdot 10^{13}$	$4.4 \pm 0.2$
Mn II	-	-	-	-	$2.2 \pm 0.2 \cdot 10^{11}$	"	$1.8 \pm 0.2 \cdot 10^{11}$	"
Mg II	$3.4 \pm 0.2 \cdot 10^{11}$	$1.8 \pm 0.2$	$1.5 \pm 0.1 \cdot 10^{12}$	$6.5 \pm 0.2$	$3.1 \pm 0.6 \cdot 10^{13}$	$3.8 \pm 0.2$	$5.9 \pm 0.8 \cdot 10^{13}$	$4.6 \pm 0.2$
Mg I	$\leq 3 \cdot 10^9$	-	$\leq 1 \cdot 10^{10}$	-	$8.0 \pm 0.6 \cdot 10^{10}$	"	$2.5 \pm 0.3 \cdot 10^{11}$	"
Si II	-	-	-	-	$5.8 \pm 0.5 \cdot 10^{13}$	$3.75 \pm 0.25$	$7.5 \pm 0.3 \cdot 10^{13}$	$4.5 \pm 0.3$
Al III	-	-	-	-	$1.9 \pm 0.3 \cdot 10^{11}$	"	$1.8 \pm 0.6 \cdot 10^{11}$	"
Si III	-	-	-	-	$\leq 5 \cdot 10^{12}$	"	$(1.5 - 10) \cdot 10^{14}$	"
S II	-	-	-	-	$1.1 \pm 0.4 \cdot 10^{14}$	"	$2.3 \pm 0.5 \cdot 10^{14}$	"
N I	-	-	-	-	$5.5 \pm 0.8 \cdot 10^{13}$	$4.6 \pm 0.6$	$2.6 \pm 0.5 \cdot 10^{13}$	$5.5 \pm 0.7$

area of the spectrum free of any stellar lines and the continuum is therefore also very easy to determine. Because of the similarity of iron and manganese masses and with the assumption that Fe II and Mn II come from regions of the same temperature and turbulent velocity, we assume  $b(\text{Fe II})=b(\text{Mn II})$  for C and D and fit these four lines simultaneously.

### 3.1.2. The Mg II and Mg I lines

The Mg II lines are strongly saturated. It is thus in principle difficult to derive column densities and  $b$ -values from the line profile fitting. However, with the assumption that  $b(\text{Mg II})=b(\text{Mg I})$ , which is true if Mg I and Mg II arise from the same regions, the two Mg II lines can be fitted simultaneously with the unsaturated Mg I line. Since the structure of the sight-line is known from the analysis of the Fe II lines, the positions of all components in the Mg II profiles can be determined precisely from the position of component A which is clearly visible in the spectra. Mg I and Mg II column densities and  $b$ -values could thus be derived for all components from the simultaneous fit of all the lines of the two species.

### 3.1.3. The Si II and Al III lines

The Si II 1808 line is weak but the C and D components are clearly identified. It is located in a portion of the spectrum with many narrow stellar lines. It is thus difficult to determine accurately the stellar continuum. But the silicon  $b$ -value must be between that of iron and that of magnesium, i.e.  $b(\text{Si II})=3.5 - 4.0 \text{ km s}^{-1}$  for cloud C and  $b(\text{Si II})=4.2 - 4.8 \text{ km s}^{-1}$  for cloud D. With these constraints on the  $b$ -values only the deepest stellar profiles are permitted by the fit and the column density uncertainties are thereby considerably reduced.

In both Al III lines, which appear in the same spectrum at 1854.7 and 1862.8 Å, two small features separated by  $\simeq 10.5 \text{ km s}^{-1}$  are detected at the bottom of the strong stellar lines. Since the atomic mass of aluminium is close to that of silicon, we adopt the Si II  $b$ -values to fit the Al III lines.

### 3.2. The G160M data

Many important species only show absorption lines below 1800 Å. This is the case for neutrals like N I, O I and H I as well as medium or highly ionized species like S II, C II, Si III, Si IV and C IV. Unfortunately, the Ech-A was not available at the time of the observations and the data were taken using the G160M grating with a lower resolution than the echelle gratings. With a resolution element of about  $15 \text{ km s}^{-1}$ , the different components seen in the Ech-B spectra are not resolved. An additional difficulty comes from the low rotational velocity of  $\beta$  CMA ( $v \sin i \sim 30 \text{ km s}^{-1}$ ) which implies relatively narrow stellar lines, sometimes not easily differentiated from the interstellar contribution. Nevertheless, for most species the total sight-line column density has been derived by fitting the interstellar absorption with one component and for N I, S II and Si III, a multi-components fit was possible. Figure 2 shows some of the interstellar lines observed with G160M together with the best fits, and Table 3 summarizes the derived column densities.

#### 3.2.1. Velocity calibration

As mentioned in Sect. 2, the G160M spectra hold an uncertainty in the wavelength position of about one resolution element i.e.  $\sim 15 \text{ km s}^{-1}$ . However the velocity calibration has been improved with the help of the Si II lines, since Si II lines are present in one Ech-B spectrum (giving a precision

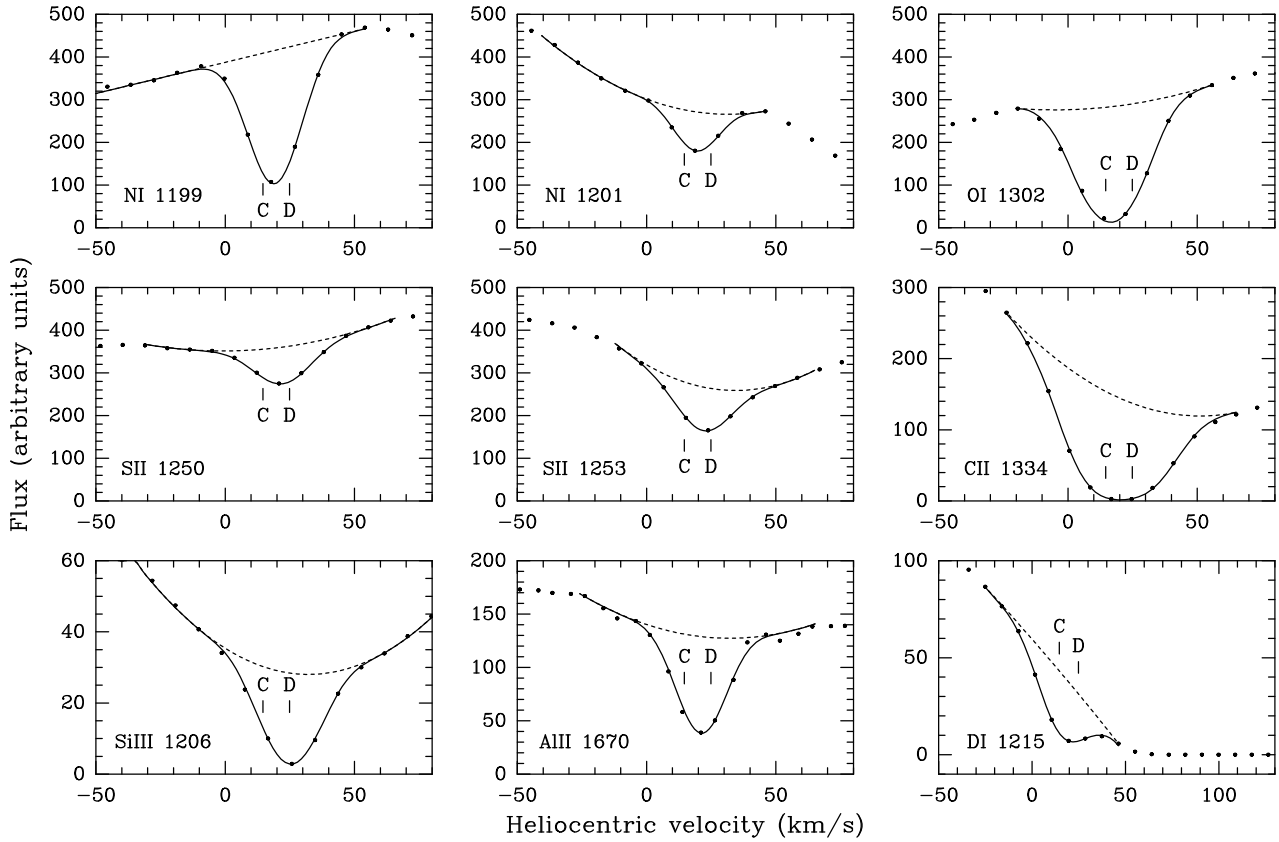


**Fig. 2.** Same as Fig. 1 for the G160M spectra of  $\beta$  CMa ( $R \sim 20\,000$ ). The column densities used for the fits are given in Table 3. Although the position of components C and D are indicated in all spectra, the fits were performed with a one-component model except for NI, S II and Si III.

**Table 3.** Total sight-line column densities ( $\text{cm}^{-2}$ ) derived from the G160M spectra.

NI	$0.9 - 1.1 \cdot 10^{14}$
O I	$\geq 5.5 \cdot 10^{14}$
D I	$\geq 2.5 \cdot 10^{13}$
Al II	$5.0 - 8.0 \cdot 10^{12}$
S II	$3.1 - 3.7 \cdot 10^{14}$
C II	$\geq 4 \cdot 10^{14}$
Si III	$1.5 - 10 \cdot 10^{14}$
Si IV <sup>1</sup>	$\leq 1.7 \cdot 10^{11}$ ( $\leq 2.7 \cdot 10^{11}$ )
S III <sup>2</sup>	$0.9 - 2.1 \cdot 10^{13}$

<sup>1</sup>  $3\sigma$  upper limit for  $b = 7 \text{ km s}^{-1}$  ( $b = 11 \text{ km s}^{-1}$ )

<sup>2</sup> from Copernicus data, see Sect. 5.1

of  $3 \text{ km s}^{-1}$ ) and in four of the six G160M spectra (see Table 1). The convolution of the theoretical profile obtained for the high resolution Si II 1808 line with the G160M line spread function gives a blended feature centered at a ve-

locity of  $20.5 \text{ km s}^{-1}$ . This velocity is therefore adopted for the center of the interstellar Si II absorption lines in the four G160M spectra, yielding a wavelength calibration of these spectra with the accuracy of the Ech-B spectra. The velocity shifts thereby applied to the four G160M spectra rank from 2.5 to  $12.5 \text{ km s}^{-1}$ , which are within the nominal precision of the data.

### 3.2.2. The velocity-ionization relationship

Figure 3 shows the central velocity of the absorption (from the one-component fit of the line) versus the ionization potential, for all species for which a good calibration has been obtained via the above process. It shows that, as the ionization potential increases from DI to Si III, the central velocity of the absorption profile increases from a velocity intermediate to components C and D up to the velocity of component D, with a small departure for O I and C II which are saturated. This implies that component D contributes more than component C to the ionized species

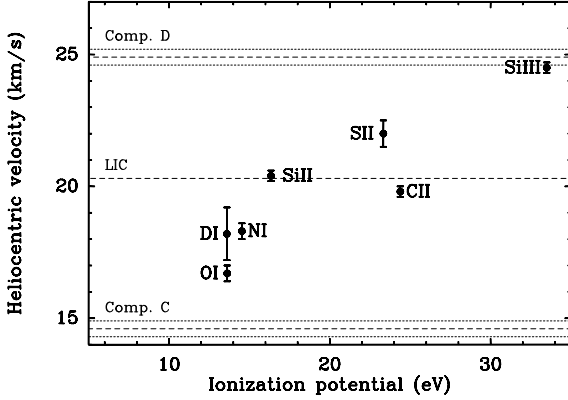


**Fig. 3.** Central velocity of the G160M interstellar features versus the ionization potential of the elements. The dashed and dotted lines show the velocity positions of the clouds together with their relative uncertainty. The  $\pm 1.5 \text{ km s}^{-1}$  absolute error on the velocities is not shown since it affects all clouds simultaneously.

absorption and component C contributes more than component D to the neutrals absorption.

In the following section we give some details on the analysis of each species. Special care has been put in trying to extract information on the distribution of matter between the two main components, although it is not always feasible at the G160M resolution.

### 3.2.3. Neutral species : N I, O I, H I and D I

Three N I lines are available in our data at 1199.5, 1200.2 and 1200.7 Å. The fact that the three lines have different oscillator strengths, with at least one of them unsaturated, permits an accurate one-component fit, giving the following total line-of-sight N I column density and  $b$ -value :  $N(\text{N I}) = 1.0 \pm 0.1 10^{14} \text{ cm}^{-2}$ ,  $b(\text{N I}) = 8.5 \pm 0.3 \text{ km s}^{-1}$ .

But a multi-component fit is also performed, taking into account four components : components C and D, which contribute both to the absorption feature according to Sect. 3.2.2, as well as the LIC and component 2, the column densities of which have been derived in the line of sight of  $\epsilon$  CMA with new Ech-A data (Gry & Dupin, in prep.) and represent 25 % of the N I absorption in the  $\beta$  CMA sight-line. The three N I lines are fitted simultaneously with four components and the following constraints : the velocity of each component is fixed at the known position, the  $b$ -values and column densities for the LIC and component 2 are those found for  $\epsilon$  CMA and the  $b$ -values for components C and D are between that of Mg and that given by the maximum temperature allowed for the clouds (see Sect. 4.1).

We derive  $N(\text{N I}) = 5.5 \pm 0.8 10^{13} \text{ cm}^{-2}$ ,  $b(\text{N I}) = 4.6 \pm 0.6 \text{ km s}^{-1}$  and  $N(\text{N I}) = 2.6 \pm 0.5 10^{13} \text{ cm}^{-2}$ ,  $b(\text{N I}) =$

$5.5 \pm 0.7 \text{ km s}^{-1}$  for component C and component D, respectively.

As the only available O I line (1302 Å) is saturated, we could not find a unique solution with a multi-component model. Therefore we simply derive a column density lower limit for the total sight-line using a one-component model, and taking the largest  $b$ -value that gives a reasonable fit. We find  $N(\text{O I}) \geq 5.5 10^{14} \text{ cm}^{-2}$  for  $b \leq 11.0 \text{ km s}^{-1}$ .

The saturated Lyman  $\alpha$  H I interstellar feature has large wings and it is difficult to separate it from the stellar line. Furthermore too many components have to be taken into account to allow reliable results from profile fitting. But the Lyman  $\alpha$  D I line contribution can be separated from that of H I and is only slightly saturated. We derive  $N(\text{D I}) \geq 2.5 10^{13} \text{ cm}^{-2}$ ,  $b \leq 12.0 \text{ km s}^{-1}$ .

### 3.2.4. The singly ionized species : S II, Si II, C II and Al II

Five lines of Si II at 1190, 1193, 1260, 1304 and 1526 Å are available but the line at 1190.4 Å is blended with the S III line at 1190.2 Å and cannot be used. The two-component model derived from the analysis of the Ech-B Si II 1808 line has been applied to the four available lines and gives a good fit for all of them.

The G160M data include three S II lines at 1250, 1253 and 1259 Å. The three lines have first been fitted simultaneously with one component only : this gives  $N(\text{S II}) = 3.4 \pm 0.3 10^{14} \text{ cm}^{-2}$  for the total sight-line. As these transitions are weak and the lines are not saturated, most of the absorption must be due to the largest components. The contribution of the LIC and component 2 can be estimated from their S II column densities in the  $\epsilon$  CMA sight-line : Gry & Dupin (1997) have found an upper limit of  $6 10^{12} \text{ cm}^{-2}$  for the LIC, and component 2 appears to be even weaker. These two clouds should therefore not account for more than 3% of the sulfur in the  $\beta$  CMA sight-line. The three S II lines are thus expected to be strongly dominated by the two largest components C and D. A two-component fit is thus performed, with the Si II  $b$ -values, and gives  $N(\text{S II}) = 1.1 \pm 0.4 10^{14} \text{ cm}^{-2}$  for cloud C and  $N(\text{S II}) = 2.3 \pm 0.5 10^{14} \text{ cm}^{-2}$  for cloud D. It is seen that the sum of the two cloud contributions is equal to the one-component fit result, but with a larger uncertainty.

The C II 1334 line is strong and saturated. Each component of the sight-line gives a significant contribution to the interstellar absorption feature and, as for O I, we only derive a column density lower limit :  $N(\text{C II}) \geq 4 10^{14} \text{ cm}^{-2}$  with  $b \leq 14.5 \text{ km s}^{-1}$ . The interstellar C II\*1335 line is located at the end of the spectrum and it was not possible to use it.

The Al II line at 1670 Å is located in a spectral region which does not include Si II lines and thus does not have a precise velocity calibration. It is therefore fitted with a one-component model which gives  $N(\text{Al II}) = 6.5 \pm 1.5 10^{12} \text{ cm}^{-2}$  for  $b = 6.5 \pm 0.7 \text{ km s}^{-1}$ . The large un-

certainty in the column density is due to the fact that we have only one Al II line and that the stellar continuum is not well defined at these wavelengths.

### 3.2.5. The highly ionized species : S III, Si III, Si IV and C IV

The S III line at 1190.2 Å is unfortunately severely blended with the Si II line at 1190.4 Å. Thus, no satisfactory stellar continuum could be drawn and this line was not used.

The Si III 1206 line is saturated but the stellar line is well defined and can be modelled by a parabola. The fit confirms that most of the Si III is in cloud D and with the assumption that  $b(\text{Si III})=b(\text{Si II})$ , gives  $N(\text{Si III})=1.5 - 10 10^{14} \text{ cm}^{-2}$  for cloud D and an upper limit for cloud C of  $N(\text{Si III})\leq 5 10^{12} \text{ cm}^{-2}$ . The large uncertainty on the D column density is due to the line saturation.

A spectral region containing the Si IV lines at 1393 Å and 1402 Å was observed, but no interstellar absorption feature was detected at these wavelengths. Only  $3\sigma$  upper limits are derived for the column density. If it is assumed that Si IV comes from the clouds themselves i.e.  $b(\text{Si IV})=b(\text{Si II})\sim 7 \text{ km s}^{-1}$ , the strongest line implies  $N(\text{Si IV})\leq 1.7 10^{11} \text{ cm}^{-2}$ . If Si IV is produced by a high temperature interface between the clouds and the hot surrounding medium, a  $3\sigma$  upper limit gives  $N(\text{Si IV})\leq 2.7 10^{11} \text{ cm}^{-2}$  for  $T = 2 10^5 \text{ K}$ .

Fig. 4 shows the  $\beta$  CMa spectrum between 1547 Å and 1552 Å containing the C IV 1548,1550 doublet. When the stellar lines are represented by fourth order polynomials, an absorption feature appears at the bottom of both stellar lines. Although the interstellar nature of these features is not beyond dispute they nevertheless occur in both lines at the same velocity which also happens to be the LIC velocity ( $\sim 20 \text{ km s}^{-1}$ ). In their study of the interstellar gas toward  $\epsilon$  CMa, Gry et al. (1995), reported a C IV absorption at the LIC velocity, with a width corresponding to thermal broadening at  $T = 2 10^5 \text{ K}$ . They suggest that the absorption could be due to the interface between the LIC and the hot surrounding medium. In Fig. 4, the C IV absorption lines in  $\beta$  CMa are compared to the model found for the LIC absorption in the case of  $\epsilon$  CMa ( $N(\text{C IV})=3.2 10^{12} \text{ cm}^{-2}$ ,  $T = 2 10^5 \text{ K}$ ,  $V = 20.3 \text{ km s}^{-1}$ ). The C IV data are consistent with the expected LIC absorption as determined toward  $\epsilon$  CMa.

### 3.3. Comparison with Copernicus observations

$\beta$  CMa has been observed with Copernicus (Gry et al. 1985) at shorter wavelengths and with a slightly higher resolution than that of G160M, but not sufficient to resolve the different components. The Copernicus O I and Si II column densities are compatible with the G160M values. But the N I, D I, S II and Si III column densities derived from the Copernicus observations are systematically lower than those we derive from our data. We have therefore re-

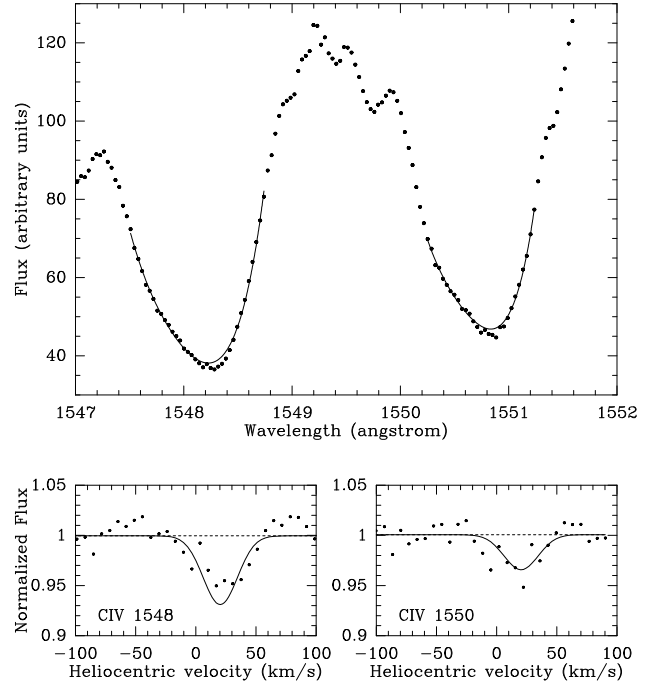


**Fig. 4.** Possible interstellar absorption in the C IV lines. *Upper* : the  $\beta$  CMa spectrum between 1548 and 1552 Å. The solid lines are fourth order polynomials fitting the stellar lines. Possible interstellar absorptions appear at the bottom of the lines. *Lower* : model of the LIC absorption found for  $\epsilon$  CMa (Gry et al. 1995) superimposed on the normalised  $\beta$  CMa spectra.

viewed the Copernicus background estimates used by Gry et al. and reached the conclusion that the contamination due to diffuse light in the Copernicus instrument may have been incorrectly estimated. This is clear in the case of the Si III line at 1206.5 Å which is undoubtedly saturated in our data (the background level is given by the bottom of the saturated Lyman  $\alpha$  line present in the same spectrum) while it does not appear saturated in the Copernicus spectrum. According to Rogerson et al. (1973), the background of the Copernicus data is roughly 25% of the continuum. If this background contribution has been underestimated, the Copernicus column density of unsaturated lines may have been underestimated by 25%. If such a correcting factor is allowed, Copernicus and G160M values are in agreement for N I and S II. Since the Si III 1206 line is saturated, the column density estimate is very sensitive to any background misplacement and the value derived from Copernicus had been more strongly underestimated.

## 4. Physical conditions in the clouds

#### 4.1. Temperature and turbulent velocity

Thanks to the mass difference between Mg and Fe, the thermal and turbulent contributions to the  $b$ -values can in principle be disentangled, providing a range of temperatures and turbulent velocities for each cloud. The  $b$ -values are listed in Table 2. For component B, the  $b$ -values found for Mg II and Fe II are so different that the ranges do not allow a measure of the turbulence. Conversely, for components A, C and D, the ranges for Mg II and Fe II overlap and as the atomic mass of these elements imposes  $b(\text{Mg II}) \geq b(\text{Fe II})$ , this only provides upper limits for the temperatures :  $T \leq 8000$  K for cloud A,  $T \leq 9500$  K for cloud C and  $T \leq 13500$  K for cloud D. The derived ranges for the turbulent velocities are the following :  $1.7 \text{ km s}^{-1} \leq V_{\text{turb}} \leq 3.3 \text{ km s}^{-1}$  for cloud A,  $3.2 \text{ km s}^{-1} \leq V_{\text{turb}} \leq 4.0 \text{ km s}^{-1}$  for cloud C and  $4.0 \text{ km s}^{-1} \leq V_{\text{turb}} \leq 4.8 \text{ km s}^{-1}$  for cloud D.

#### 4.2. Electron density

Cloud C and cloud D are both detected in Mg I and Mg II. If ionization equilibrium between Mg I and Mg II following e.g. Frisch et al. (1990) and Lallement et al. (1994) is assumed, the electron density in the clouds can be derived :  $n_e = \Gamma / (\alpha_{\text{rad}} + \alpha_{\text{die}}) * N(\text{Mg II}) / N(\text{Mg I}) - (k_{\text{exch}} + C)$  ; where the Mg II radiative recombination rate ( $\alpha_{\text{rad}}$ ) is taken from Aldrovandi & Péquignot (1973), the dielectronic recombination rate ( $\alpha_{\text{die}}$ ) from Nussbaumer & Storey (1986), the Mg I ionization rate by charge exchange with protons ( $k_{\text{exch}}$ ) from Allan et al. (1988), and the Mg I radiative ionization rate ( $\Gamma$ ) from Phillips et al. (1981).  $C$  is the Mg I collisional ionization rate but it is negligible at the temperatures involved. For a warm cloud typical temperature of  $T \sim 7000$  K, the range of  $N(\text{Mg II})/N(\text{Mg I})$  values derived from the observations implies  $n_e = 0.18 - 0.54 \text{ cm}^{-3}$  for cloud C and  $n_e = 0.38 - 1.82 \text{ cm}^{-3}$  for cloud D.

### 5. Ionization of the clouds

#### 5.1. The ionization degree

Sulfur is a good element to use to derive the total hydrogen abundance because it is only slightly (Harris & Mas Hesse 1986) or not (Sofia et al. 1994) depleted in the interstellar gas. We thus apply the solar abundance given by Anders & Grevesse (1989),  $\log[N(\text{S})/N(\text{H})] = -4.73$ , to our determined sulfur column densities to derive the total hydrogen column density in the main components C and D. The S III column density is taken from Gry et al. (1985),  $N(\text{S III}) = 0.9 - 2.1 \cdot 10^{13} \text{ cm}^{-2}$ , after correction for the likely background misplacement as explained in Sect. 3.3. Most of the S III is assumed to be in component D, as is Si III (see Sect. 3.2.5), thus for cloud D, the total column density is derived from the sum of S II and S III column densities :  $N(\text{H}_{\text{tot}}) = 1.0 - 1.6 \cdot 10^{19} \text{ cm}^{-2}$ . For cloud C, the S II column yields  $N(\text{H}_{\text{tot}}) = 3.7 - 8.0 \cdot 10^{18} \text{ cm}^{-2}$ .

For the total sight-line, the sum of the total sight-line S II column density and the above S III column density gives  $N(\text{H}_{\text{tot}}) = 1.7 - 2.1 \cdot 10^{19} \text{ cm}^{-2}$ . Cassinelli et al. (1996) have derived  $N(\text{He I}) \geq 1.4 \cdot 10^{18} \text{ cm}^{-2}$  from the He I 504 Å line. With a cosmic abundance of 0.1 for He this implies  $N(\text{H}_{\text{tot}}) \geq 1.4 \cdot 10^{19} \text{ cm}^{-2}$  which is in agreement with our value.

The neutral hydrogen column density toward  $\beta$  CMA has been estimated by Gry et al. (1985) by fitting the Lyman- $\beta$  profile observed with Copernicus. They found  $N(\text{H I}) = 1.6 \pm 0.6 \cdot 10^{18} \text{ cm}^{-2}$ . Recently, Cassinelli et al. (1996), using EUVE observations, have modelled the stellar spectrum and found an interstellar neutral hydrogen absorption of  $N(\text{H I}) = 2.0 \pm 0.2 \cdot 10^{18} \text{ cm}^{-2}$ , which is in good agreement with the previous estimate.

If we adopt the wider range for  $N(\text{H I})$ , the neutral fraction is  $N(\text{H I})/N(\text{H}_{\text{tot}}) = 0.05 - 0.13$  for the total line of sight. This implies that about 90% of the matter of the sight-line is ionized.

The share of neutral hydrogen between the main components is difficult to assess. As seen in Table 2, the way N I is distributed over the main components is very different from the way Mg II is distributed, although the ionization potentials of the two elements are close (14.5 and 15.0 eV) : the column density ratio between C and D is close to 2 for N I and close to 1/2 for Mg II. This suggests that the share of neutral hydrogen between C and D cannot be derived from that of neutral nitrogen. Nevertheless, since component D is in general the more ionized, and since the N I ionization potential is slightly larger than that of H I, it is likely that the fraction of H I contained in D does not exceed the fraction of N I, which is 20% to 30% of the total neutral nitrogen in the line of sight (Sect. 3.2.3). It is thus likely that no more than 30% of the total neutral gas lies in cloud D :  $N(\text{H I}) \leq 6.6 \cdot 10^{17} \text{ cm}^{-2}$ . This gives  $N(\text{H I})/N(\text{H}_{\text{tot}}) \leq 7\%$  for D.

As for component C, what we can safely say is that it does contain a good fraction of the neutral gas since the D I and O I features are centered at a velocity close to that of component C, and that it contains no more H I than that present in the total line of sight. This implies that cloud C is partially ionized with  $N(\text{H I})/N(\text{H}_{\text{tot}}) \leq 60\%$ .

#### 5.2. Origin of the ionization

Table 4 summarizes all the information available on ionization ratios in the clouds or in the line of sight as a whole. The case of hydrogen has been discussed above. For sulfur, since all S III is assumed to be in cloud D,  $N(\text{S II})/N(\text{S III})$  is derived for cloud D only. For iron and magnesium, upper limits for their total gas phase abundances  $N(\text{X})_g$  were derived by adopting the minimum depletion values found in the interstellar medium as given by Fitzpatrick (1996, 1997). Then upper limits on their second ion column density were derived by  $N(\text{X III}) = N(\text{X})_g - N(\text{X II})$ . This yields lower limits for the ratios



**Table 4.** Ionization ratios derived from the observations and from the collisional ionization model of Sutherland & Dopita (1993).

Ratios	observed		Sutherland & Dopita (1993)			
	C	D	$T=15\,000\text{ K}$	$T=20\,000\text{ K}$	$T=25\,000\text{ K}$	$T=30\,000\text{ K}$
H I/H II	$\leq 1.5$	$\leq 0.07$	1.79	$7.2 \cdot 10^{-2}$	$1.2 \cdot 10^{-2}$	$3.4 \cdot 10^{-3}$
Si II/Si III	$\geq 10.6$	$0.07 - 0.52$	47	1.1	0.17	$8.5 \cdot 10^{-2}$
Si III/Si IV	-	$\geq 600$	-	$3.8 \cdot 10^4$	648	60
Si II/Si IV	$\geq 288$	$\geq 212$	-	$4.1 \cdot 10^4$	134	5.46
S II/S III	-	$8.6 - 33$	5300	30.4	3.1	1.0
Fe II/Fe III	$\geq 0.14$	$\geq 0.05$	19.6	0.52	0.13	$7 \cdot 10^{-2}$
Mg II/Mg III	$\geq 0.20$	$\geq 0.20$	7.7	0.24	$3.3 \cdot 10^{-2}$	$9.3 \cdot 10^{-3}$
N I/N II	$\geq 0.09$	$\geq 0.02$	18.8	0.18	$2.9 \cdot 10^{-2}$	$1.2 \cdot 10^{-2}$
Al II/Al III	$\leq 50$	$\leq 67$	$2.1 \cdot 10^3$	62.4	8.8	2.38

$N(\text{X II})/N(\text{X III})$ . For nitrogen, we proceed similarly but with the first and second ion column densities. For aluminium, upper limits on the  $N(\text{Al II})/N(\text{Al III})$  ratio are derived taking the total sight-line Al II column density as an upper limit on the individual cloud Al II column densities. For silicon, the ionization ratios are derived directly from the data, taking the same upper limit for the Si IV column densities of the individual clouds as that derived for the total Si IV column density.

In principle these ionization ratios allow a discussion of the ionization mechanisms involved in the gas.

The most straightforward mechanism is photoionization by the star  $\beta$  CMa as well as its neighbour  $\epsilon$  CMa which is, as already mentioned, the strongest ionizing source in the Solar neighbourhood (Vallerga & Welsh 1995). But the comparison of our ionization ratios with models and other observations found in the literature is not really conclusive.

In general, H I regions are dominated by singly ionized species like Si II, S II and Al II while photoionized H II regions show strong absorptions in Si IV, S III and Al III (e.g. Fitzpatrick & Spitzer 1994, Spitzer & Fitzpatrick 1995, Jenkins & Wallerstein 1996, Savage & Sembach 1996a,b). The  $\beta$  CMa line of sight main components are thus atypical because, while hydrogen is substantially ionized, S II, Al II and Si II (for cloud C) or Si III (for cloud D) are still dominant and Si IV is too weak to be detected. Cowie et al. (1981), in a study of the origin and the distribution of C IV and Si IV with 46 O-B stars observed with IUE, found that almost all stars are associated with C IV and Si IV column densities of  $\sim 10^{13}\text{ cm}^{-2}$ . They conclude that most of this absorption arises in photoionized H II regions. They also present a simple photoionization model predicting the H II regions C IV and Si IV column densities. For a 25 000 K effective temperature star and an electron density of  $1\text{ cm}^{-3}$  it gives  $N(\text{C IV})= 2.6 \cdot 10^{10}\text{ cm}^{-2}$  and  $N(\text{Si IV})= 3.7 \cdot 10^{12}\text{ cm}^{-2}$  the latter being a factor of 10

higher than the  $\beta$  CMa upper limit. The model gives values compatible with the  $\beta$  CMa data for electron densities of  $0.01\text{ cm}^{-3}$  or less, much smaller than the range of values we derive (see Sect. 4.2).

York (1983) found evidence for H II regions in the line of sight to  $\lambda$  Sco (B2 IV), for which he compared the ionization ratios with those given by photoionization models with radiation fields of stars of different effective temperatures. For the effective temperature of  $\beta$  CMa ( $\sim 25\,000\text{ K}$ , Cassinelli et al. 1996), he quotes the results from Thuan (1975) for an electron density of  $0.1\text{ cm}^{-3}$ :  $\text{S II/S III}= 8$  and  $\text{Si II/Si III}= 1.6$ . In component C, Si II is clearly less ionized than in the model. For component D S II/S III is compatible with the quoted model value and Si II is somewhat more ionized, which could be explained in view of the EUV excess of  $\beta$  CMa and  $\epsilon$  CMa. On the other hand, Spitzer & Fitzpatrick (1995) have identified a photoionized H II region toward HD 149881, a halo star of similar spectral type (B0.5 III), where S II/S III is less than 1, i.e. similar to that of 'typical' H II regions around hotter stars (e.g. the three H II regions detected in the line of sight of the O9I+WC8 star  $\gamma^2$  Velorum by Fitzpatrick & Spitzer 1994) and significantly lower than the ratio we measure for component D.

Clearly the comparison of all these observations shows that a more detailed ionization model by the stars is required before any conclusion can be drawn. However, detailed photoionizing models by these two sources which take into account their EUV excess evidenced by EUVE (Cassinelli et al. 1995, Cassinelli et al. 1996) is beyond the scope of this paper.

Our ionization ratios can also be compared with those given by collisional ionization. The comparison in Table 4 with the ratios given for various equilibrium temperatures in the model of Sutherland & Dopita (1993) shows that for component D there is an agreement for all ratios for temperatures around  $T \sim 21\,000\text{ K}$ . For component C,

**Table 5.** Gas phase abundances in the clouds and for the total sight-line

	[C/H]	[N/H]	[O/H]	[Mg/H]	[Si/H]	[Al/H]	[Mn/H]	[Fe/H]
cloud C	-	$\geq -0.5$	-	$\geq -1.1$	$-0.55^{+0.23}_{-0.18}$	$\leq -0.13$	$\geq -1.13$	$\geq -1.37$
cloud D	-	$\geq -0.55$	-	$\geq -1.1$	$+0.15^{+0.33}_{-0.56}$	$\leq -0.57$	$\geq -1.53$	$\geq -1.76$
total	$\geq -1.28$	$-0.25^{+0.24}_{-0.15}$	$\geq -0.52$	$\geq -1.00$	$+0.02^{+0.26}_{-0.45}$	$-0.92^{+0.14}_{-0.16}$	$\geq -1.30$	$\geq -1.49$

although the temperature ranges derived from Si II/Si III and Al II/Al III do not overlap, the ratios point to temperatures ranging from about 16 000 K to about 22 000 K. For both components, these temperatures are significantly higher than the kinetic temperatures of the clouds derived from profile fitting (Sect. 4.1). Thus if the clouds are collisionally ionized, they cannot be in equilibrium, which indicates that they are still in a cooling and recombining phase.

Trapero et al. (1996) in their study of halo high velocity clouds (HVCs) with the GHRS also proposed that the ionization of several HVCs in the line of sight to 23 Ori and  $\tau$  CMA is due to collisional ionization. As in the case of the clouds in the  $\beta$  CMA sight-line they are not in ionization equilibrium and are overionized with respect to their kinetic temperatures : the ionization balance corresponds to a collisional ionization equilibrium near  $T = 25\,000$  K while the temperature derived from the Mg II lines is  $\leq 12\,000$  K. Trapero et al (1996) suggest that the HVCs consist of already cooling warm ionized gas, originally probably collisionally ionized and heated by a shock. Our results tend to support this interpretation for components C and D, in view of the depletion results which are discussed in Sects. 6 and 7.

## 6. Gas phase abundances

The gas phase abundance of an element X relative to H is defined by

$$\left[\frac{X}{H}\right] = \log \left[\frac{N(X)}{N(H)}\right] - \log \left[\frac{N(X)}{N(H)}\right]_{\text{cosmic}}$$

where  $\log [N(X)/N(H)]_{\text{cosmic}}$  is the solar abundance as given by Anders & Grevesse (1989).

All available [X/H] derived from our study are listed in Table 5. When possible their values for components C and D are listed separately. All relevant ionization stages are considered and when applicable (Si and Al) we use the sum of the various stage column densities.  $N(\text{O I})$  is compared to  $N(\text{H I})$ , as is  $N(\text{N I})$  for consistency with other studies although in the case of N I, as mentioned in Sect. 5.1, some ionization effects might be involved. All other element column densities are compared to total hydrogen column density. As Si III is the dominant stage in component D, it is probable that Fe III, Mg III and Mn III are

also significant. This is why in Table 5 the gas phase abundance of their singly ionized form is listed as a lower limit only.

It appears that in cloud D silicon is not at all, or only slightly, depleted. Its gas phase abundance is at least 0.44 dex higher than the value given in the Table 5 of Jenkins & Wallerstein (1996) for the depleted low velocity gas in the disk. In their Fig. 6, Savage & Sembach (1996a) have plotted the mean gas phase abundances of several elements for different ISM components found in the disk and in the halo. The value we find for silicon is the one they quote for the warm diffuse gas in the halo. In this component, most of the silicon is in the double ionized form (Si III/Si II = 2 – 14). The ionization potentials of Fe II, Mn II and Mg II being lower than that of Si II, it is expected that in cloud D, Fe III, Mn III and Mg III are at least two times more abundant than Fe II, Mn II and Mg II. The gas phase abundances we derive for iron, manganese and magnesium are thus, as for silicon, the same as those quoted for the halo gas in the Fig. 6 of Savage & Sembach (1996a).

In cloud C, the silicon and the iron gas phase abundances are at least 0.12 and 0.13 dex higher respectively than the values of the depleted low velocity gas in the disk (Jenkins & Wallerstein 1996). The silicon gas phase abundance corresponds to that of the warm gas in the disk in Fig. 6 of Savage & Sembach (1996a) and is within the error bars of that of the halo gas. In cloud C, silicon is mostly in its singly ionized form. We thus assume the same is true for iron, manganese and magnesium, for which as silicon, the gas phase abundances thus also correspond to those of the warm gas in the disk and are within the error bars of those of the halo gas.

For the other elements, gas phase abundances were derived for the total sight-line only.

The abundance of nitrogen,  $[N/H] = -0.25^{+0.24}_{-0.15}$ , is in good agreement with previous values derived from Copernicus observations toward many stars :  $-0.26^{+0.24}_{-0.34}$  (Ferlet, 1981), and  $-0.29^{+0.15}_{-0.10}$  (York et al., 1983), as well as with the recent determination by Meyer et al. (1998a) with the GHRS at high resolution :  $-0.17^{+0.02}_{-0.03}$ .

For oxygen, our lower limit  $[O/H] \geq -0.52$  is compatible with Copernicus results of  $[O/H] = -0.39^{+0.24}_{-0.10}$  (York et al. 1983, Keenan et al. 1985) and very close to the Meyer et al. (1998b) accurate determination of  $-0.43 \pm 0.02$ , which is only 0.09 higher. If Meyer's value is applicable to the

**Table 6.** C and D cloud characteristics derived from the observations.

cloud	C	D
$V_{\text{helio}}$ (km s $^{-1}$ )	14.5	25
$V_{\text{LSR}}$ (km s $^{-1}$ )	-5.0	5.5
$T$ (K)	$\leq 9500$	$\leq 13\,500$
$V_{\text{turb}}$ (km s $^{-1}$ )	3.2 – 4.0	4.0 – 4.8
$N(\text{H}_{\text{tot}})$ (cm $^{-2}$ )	$3.7 - 8.0 \cdot 10^{18}$	$1.0 - 1.6 \cdot 10^{19}$
$N(\text{H I})/N(\text{H}_{\text{tot}})$	$\leq 0.60$	$\leq 0.07$
$n_e$ (cm $^{-3}$ ) <sup>1</sup>	0.18 – 0.54	0.38 – 1.82

<sup>1</sup> from Mg I/Mg II, assuming ionization equilibrium and  $T=7000$  K

$\beta$  CMA sight-line this implies that its O I column density should not exceed  $7.3 \cdot 10^{14}$  cm $^{-2}$ .

For carbon, the lower limit derived from the strongly saturated C II line does not give any interesting constraint.

The aluminium abundance in the sight-line of  $\beta$  CMA is known with a rather good precision. Aluminium is found to be significantly depleted, but less than toward  $\alpha$  Vir (York & Kinahan 1979) or toward  $\lambda$  Sco (York 1983). Jenkins & Wallerstein (1996) show in their Table 5 the aluminium abundance in the gas phase for the depleted low velocity gas in the disk for  $n_e=3$  cm $^{-3}$  and  $n_e=0.1$  cm $^{-3}$ . These values are respectively  $\sim 1.7$  dex and  $\sim 0.7$  dex lower than that derived from our data. Conversely the  $\beta$  CMA value agrees with those found toward halo stars like HD 18100 (Savage & Sembach, 1996b) or HD 72089, HD 22586, HD 49798 and HD 120086 (Jenkins & Wallerstein, 1996).

Therefore it appears that both clouds have gas phase abundances corresponding to warm gas. Component C abundances are compatible with those of warm clouds in the disk, and with those of halo clouds if the amounts of Fe III, Mg III and Mn III are significant. Component D shows a depletion pattern similar to that of the halo clouds.

## 7. Similarity to other ISM components and nature of the gas

Table 6 summarizes the characteristics of components C and D derived from the observations.

Warm diffuse ionized gas is a major component of the interstellar medium in our Galaxy. It is detected mostly through pulsar dispersion measures and H $\alpha$  emission, especially at high Galactic latitudes. It is warm ( $T \sim 10\,000$  K) and like our components it presents line ratios which differ from that of classical H II regions (e.g. Reynolds 1991). The warm ionized gas is often seen to be associated with neutral gas as in the line of sight of HD 93521 where Spitzer & Fitzpatrick (1993) observed clouds where neutral and ionized gas seem to be mixed

in partially ionized clouds, as in component C. Reynolds et al. (1995) have compared H $\alpha$  and 21 cm emission in a  $10^\circ \times 12^\circ$  region of the sky away from the galactic plane and found that 30% of the H $\alpha$  emitting gas is spatially and kinematically associated with 21 cm emitting gas but show that in this case H $^0$  and H $^+$  gas occupy close but separate regions. Here again the temperature of these "H $\alpha$  emitting H I clouds" is about 8000 K, with electron densities around 0.2 cm $^{-3}$  and hydrogen ionization ratios ( $N(\text{H I})/N(\text{H}_{\text{tot}})$ ) ranging from 0.5 to 0.9. All these characteristics are comparable to those derived here, especially for component C.

The ionization mechanism of the diffuse ionized gas is still unclear (e.g. Reynolds et al. 1995). Many authors (Domgörgen & Mathis 1994, Miller & Cox 1993, Reynolds & Ogdén 1979, Mathis 1986) invoke photoionization by O stars but often note that the fact that the UV photons can reach the diffuse gas at high latitude many parsecs away without being absorbed remains a mystery. Ogdén & Reynolds (1985) use a model of a shock propagating through the ambient medium to explain the ionization of the long filament they have observed. Spitzer & Fitzpatrick (1993) mention penetrating radiation (energetic particles, X-rays) or in situ sources (dark matter decay, Sciama 1990) to explain the ionization of the H $^+$  and H $^0$  mixed clouds. Whether components C and D observed in the line of sight of  $\beta$  CMA are of comparable nature as the widespread warm ionized gas remains an open question.

Our components can also be compared to other interstellar constituents by their elemental abundances. Component D shows abundances similar to that of the high velocity halo clouds and to that of supernova remnants observed toward HD 72089 (Jenkins & Wallerstein 1996) which are known to have been shocked. As noted by Savage & Sembach (1996a), shocks are the most important process in the destruction of dust grains, and the low depletion in the halo clouds should result from the processes that inject the clouds into the halo. We suggest that cloud D could have been subjected to shocks in the past. This suggestion is supported by the ionization ratios which are compatible with collisional ionization and recombination after cooling (as in Trapero et al. 1996).

For cloud C the situation is somewhat less clear, as it is slightly more depleted than cloud D and less ionized. However cloud C has abundances similar to that of the warm disk and halo gas. It could also have been shocked, as it has ionization ratios close to those given by collisional ionization at a temperature lower than that derived for cloud D.

The characteristics of cloud C and D are also comparable to those of other local interstellar clouds. The electron density of the LIC derived by Gry et al. (1995) from the Mg II/Mg I ratio is  $n_e = .09_{-.07}^{+.23}$  cm $^{-3}$  and the central value corresponding to the preferred temperature of  $T \sim 7000$  K implies a hydrogen ionization fraction close to 50%. Wood & Linsky (1997) have derived a similar range

for the electron density of the LIC in the line of sight of Capella,  $n_e = .11_{-0.06}^{+0.12} \text{ cm}^{-3}$ , from the excited state C II column density, confirming that hydrogen is substantially ionized in the LIC.

A study of elemental abundances in the LIC has been performed through the analysis of new GHRS Ech-A data for  $\epsilon$  CMa by Gry & Dupin (1997) and suggests that the Local Cloud shows very little depletion, implying that most of the matter has been returned to the gas phase by some dust sputtering process. Another small component in the line of sight of  $\epsilon$  CMa has been analysed with the same data and its preliminary study has been presented by Dupin & Gry (1997). As in the case of our component D in the line of sight of  $\beta$  CMa, this component is warm ( $\sim 8000$  K), strongly ionized (more than 95%), and only slightly depleted. It also has ionization ratios compatible with those given by collisional equilibrium at  $T \sim 25000$  K.

These results show that this overall region of the local interstellar medium is substantially ionized and undepleted. The characteristics of the components and their similarities with diffuse high velocity halo clouds lead us to suggest that the Canis Majoris tunnel was affected by violent events in the past, perhaps related to the Local Bubble formation.

## 8. Conclusions

We have studied the nature of the ionized gas that dominates the  $\beta$  CMa sight-line. There appears to be two distinct components (named C and D) with ionization fractions greater than 40% and 90% respectively. Constraints have been derived for the depletion which are similar to those for the warm diffuse gas in both the disk and halo for component C, and to those for the high velocity halo clouds for component D. Silicon seems to be undepleted in cloud D and only slightly depleted in cloud C, which is also the case for the other elements studied.

The ionization ratios observed are roughly compatible with those given by theoretical calculations of collisional ionization equilibrium at temperatures close to 20000 K. As the kinetic temperatures of the clouds are actually a factor of two lower, we conclude that if the clouds are collisionally ionized, they are out of equilibrium. Nevertheless photoionization by  $\beta$  CMa and  $\epsilon$  CMa has not been ruled out and the data we present should be analysed with more complete photoionization models taking into account the strong EUV excess of these stars.

The processes which have led to this physical state could be the same as those which have given rise to the high velocity clouds detected in the halo. New observations of the interstellar medium in the sight-line to  $\epsilon$  CMa lead to similar conclusions for the LIC and another component detected toward this star. A shock which travelled in the past through these clouds could have ionized them and disrupted the dust grains giving rise to the ionization

and low depletion values found ; the clouds would now be recombining after cooling. Thus, the main components detected towards  $\beta$  CMa could result from the blast-wave that created the so-called Local Bubble.

*Acknowledgements.* We thank Alfred Vidal-Madjar for making the data available to us and Dan Welty for providing his profile fitting software. We are grateful to Alan Harris and to our referee K. de Boer for suggestions which led to substantial improvements on the manuscript.

## References

- Allan R.J., Clegg R.E.S., Dickinson A.S., Flower D.R., 1988, MNRAS, 235, 1245
- Anders E., Grevesse N., 1989, Geochim. Cosmochim. Acta 53, 197
- Aldrovandi S.M.V., Péquignot D., 1973, A&A 25, 137
- Bergeson S.D., Lawler J.E., 1993, ApJ 414, L137
- Bruhweiler F.C., Cheng K.P., 1988, ApJ 355, 188
- Cassinelli J.P., Cohen D.H., Mac Farlane et al., 1995, ApJ 438, 932
- Cassinelli J.P., Cohen D.H., Mac Farlane et al., 1996, ApJ 460, 949
- Cowie L.L., Taylor W., York D.G., 1981, ApJ 248, 528
- Domgörgen H., Mathis J.S., 1994, ApJ 428, 647
- Cox D.P., Reynolds R.J., 1987, ARA&A 25, 203
- Duncan D., 1992, Goddard High Resolution Spectrograph Instrument Handbook, version 3.0, Space Telescope Science Institute
- Dupin O., Gry C., 1997, in IAU Coll. 166, The Local Bubble and Beyond, eds Breitschwerdt D. & Freyberg M. (Springer, Heidelberg), Lect. Notes in Phys. vol. 506
- Ferlet R., Laurent C., Vidal-Madjar A., York D.G., 1980a ApJ, 235, 478
- Ferlet R., Vidal-Madjar A., Laurent C., York D.G., 1980b ApJ, 242, 576
- Ferlet R., 1981, A&A 98, L1
- Fitzpatrick E.L., 1996, ApJ 473, L55
- Fitzpatrick E.L., 1997, ApJ 482, L199
- Fitzpatrick E.L., Spitzer L., 1994, ApJ 427, 232
- Frisch P.C., York D.G., 1983, ApJ 271, L59
- Frisch P.C., Welty D.G., York D.G., Fowler J.R., 1990, ApJ 357, 514
- Gry C., York D.G., Vidal-Madjar A., 1985, ApJ 296, 593
- Gry C., Lemonon L., Vidal-Madjar A., Lemoine M., Ferlet R., 1995, A&A 302, 497
- Gry C., Dupin O., 1997, in IAU Coll. 166, The Local Bubble and Beyond, eds Breitschwerdt D. & Freyberg M. (Springer, Heidelberg), Lect. Notes in Phys. vol. 506
- Harris A.W., Mas Hesse J.M., 1986, ApJ 308, 240
- Jenkins E.B., Wallerstein G., 1996, ApJ 462, 758
- Keenan F.P., Hibbert A., Dufton P.L., 1985, A&A 147, 89
- Lallement R., Bertin P., 1992, A&A 266, 479
- Lallement R., Bertin P., Ferlet R., Vidal-Madjar A., Bertaux J.L., 1994, A&A 286, 898
- Mathis J.S., 1986, ApJ 301, 423
- Meyer D.M., Cardelli J.A., Sofia U.J., 1998a, ApJ (in press)
- Meyer D.M., Jura M., Cardelli J.A., 1998b, ApJ (in press)
- Miller W.W., Cox D.P., 1993, ApJ 417, 579

- Morton D.C., 1991, ApJS 77, 119  
Nussbaumer H., Storey P.J., 1986, A&AS 64, 545  
Ogden P.M., Reynolds R.J., 1985, ApJ 290, 238  
Phillips A.P., Gondhalekar P.M., Blades J.C., 1981, MNRAS 195, 485  
Reynolds R.J., Ogden P.M., 1979, ApJ 229, 942  
Reynolds R.J., 1991, in IAU Symp. 144, The Interstellar Disk-Halo Connection in Galaxies, ed Bloemen H., (Kluwer, Dordrecht), 67  
Reynolds R.J., Tuftte S.L., Kung D.T., McCullough P.R., Heiles C., 1995, ApJ 448, 715  
Rogerson J.B., Spitzer L., Drake J.F., et al., 1973, ApJ 181, L97  
Savage B.D., Sembach K.R., 1996a, ARA&A 34, 279  
Savage B.D., Sembach K.R., 1996b, ApJ 470, 893  
Sciama D.W., 1990, ApJ 364, 549  
Sofia U.J., Cardelli J.A., Savage B.D., 1994, ApJ 430, 650  
Spitzer L., Fitzpatrick E.L., 1993, ApJ 409, 299  
Spitzer L., Fitzpatrick E.L., 1995, ApJ 445, 196  
Sutherland R.S., Dopita M.A., 1993, ApJS 88, 253  
Thuan T.X., 1975, ApJ 198, 307  
Trapero J., Welty D.E., Hobbs L.M., et al., 1996, ApJ 468, 290  
Vallerga J.V., Welsh B.Y., 1995, ApJ 444, 702  
Vidal-Madjar A., Laurent C., Bonnet R.M., York D.G., 1977, ApJ 211, 91  
Welsh B.Y., 1991, ApJ 373, 556  
Welsh B.Y., Craig N., Vedder P.W., Vallerga J.V., 1994, ApJ 437, 638  
Welty D.E., Hobbs L.M., York D.G., 1991, ApJS 75, 425  
Wood B.E., Linsky J.L., 1997, ApJ 474, L39  
York D.G., 1983, ApJ 264, 172  
York D.G., Kinahan B.F., 1979, ApJ 228, 127  
York D.G., Spitzer L., Bohlin R.C., Hill J., Jenkins E.B., Savage B.D., Snow T.P., 1983, ApJ 266, L55